Supporting Online Information for "Dispersion of Solute by Electrokinetic Flow through Post Arrays and Wavy-Walled Channels"

J.J. Kirchner and E.F. Hasselbrink, Jr.*
Dept. of Mechanical Engineering
University of Michigan
Ann Arbor, MI 48109-2125

July 2, 2004

1 Flow solution and validation

The computational domain is mapped as shown in Fig. 1(b). The domain is then a simple square and boundary conditions and gridding become very easy to apply. This also has significant advantages in the scalar transport simulations, as will be evident momentarily. In this formulation the governing equations are:

$$\nabla^2_{\phi\psi} x(\phi,\psi) = 0 = \nabla^2_{\phi\psi} y(\phi,\psi), \tag{1}$$

where the subscript $\phi\psi$ denotes derivatives in (ϕ,ψ)-space.

The mapping from (ϕ,ψ)- to (x,y)-space is obtained from the derivatives:[1]

$$\frac{\partial\phi}{\partial x} = \frac{1}{J}\frac{\partial y}{\partial\psi}, \quad \frac{\partial\phi}{\partial y} = -\frac{1}{J}\frac{\partial x}{\partial\psi}, \tag{2}$$

$$\frac{\partial\psi}{\partial y} = \frac{1}{J}\frac{\partial x}{\partial\phi}, \quad \frac{\partial\psi}{\partial x} = -\frac{1}{J}\frac{\partial y}{\partial\phi}, \tag{3}$$

where the Jacobian J is the determinant of the Jacobian matrix $\boldsymbol{J}$ (note that $J = 1/|\boldsymbol{u}|^2$)

$$J = \left|\frac{\partial(x,y)}{\partial(\phi,\psi)}\right| = \begin{vmatrix} \frac{\partial x}{\partial\phi} & \frac{\partial x}{\partial\psi} \\ \frac{\partial y}{\partial\phi} & \frac{\partial y}{\partial\psi} \end{vmatrix}. \tag{4}$$

In order to solve these equations, our initial approach was, given $f_{\mathrm{bot}}(x)$ and $f_{\mathrm{top}}(x)$, to solve Eqs. 1 with a second-order central difference scheme and first-order differencing to approximate Neumann boundary conditions.[2] The linear system of equations produced by the second-order central difference scheme is block-tridiagonal and can be solved using the Block-Thomas algorithm.[3] The Cauchy-Riemann conditions were also solved using a second-order central difference scheme, and along the boundary

*Corresponding author: efhass@engin.umich.edu (734) 647-7859

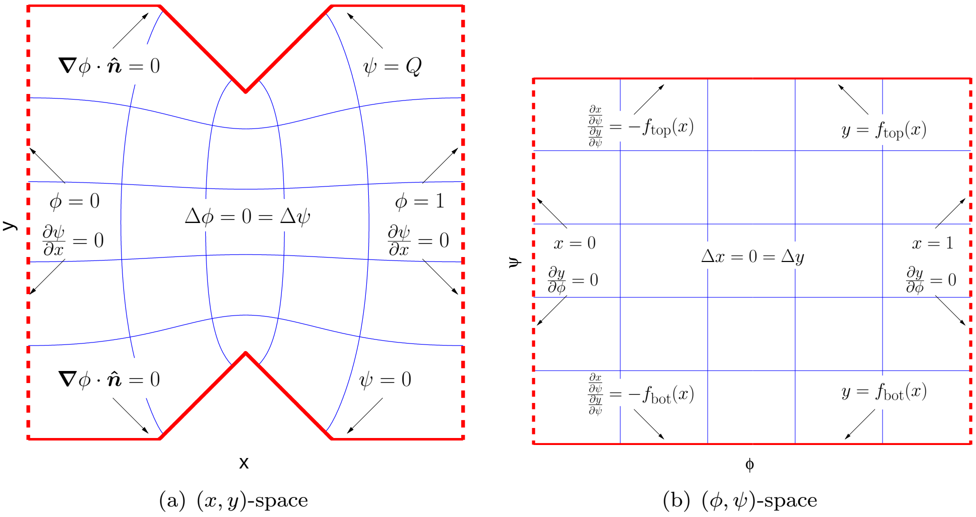

Figure 1: Diagram of governing equations and boundary conditions for an example geometry (one unit cell of in-phase diamond-shaped posts).

where a symmetric stencil was not possible, a second-order asymmetric difference scheme was used.[4] The equations for the x- and y-fields are coupled through the top and bottom boundary conditions, so the matrix equations for each were solved iteratively until the residual is less than $O[10^{-10}]$) on a 301×301 grid.[5,6]

However, in some geometries, this method was found to be subject to numerical instabilities near sharp corners where singularities exist in the exact solution. Appropriate numerical techniques to suppress these instabilities were employed, but we desired to confirm the final results using an alternative method. For these geometries, conformal mapping via the Schwarz-Christoffel transformation proved to be much more robust.[7–13] Since the transformation is defined only for polygonal geometries, squares and diamonds were defined exactly but circles are approximated by polygons made of 64 equal line segments. Values of the x- and y-fields for a regular grid of ϕ- and ψ-values were thus be found $x + iy = f(\phi + i\psi)$ on a 601×601 grid. Solutions were validated by testing the orthogonality of x- and y-fields ($\nabla_{\phi\psi} x \cdot \nabla_{\phi\psi} y = 0$), which show relative deviations $O[10^{-3}]$, with most of the error in both cases occurring near regions where the boundary changes rapidly. Flowrates obtained with the two methods were in agreement to within 1% in all cases; the Schwartz-Christoffel solution was used in all cases shown in the paper.

2 Solute transport solution and validation

Particle transport is modelled using a split-step convection-diffusion scheme.[14] The convection-step is approximated by a total differential

$$\delta\phi = \frac{\partial\phi}{\partial x}\delta x + \frac{\partial\phi}{\partial y}\delta y = \nabla\phi \cdot \delta\boldsymbol{x}, \tag{5}$$

Recognizing that $\delta\boldsymbol{x} = \boldsymbol{u}\delta t$,this is $\delta\phi = |\boldsymbol{u}|^2 \delta t$. Recalling $J = 1/|\boldsymbol{u}|^2$, the convection step is $\delta\phi = \mathrm{Pe} \cdot \delta t/J$, where the Péclet number $\mathrm{Pe} = (\Delta\phi_x/\Delta x)h/D_{12}$ is a non-dimensional velocity scale.

The length of the diffusion step r_{xy} is calculated from a normal distribution with $\sigma = \sqrt{4\delta t}$, the factor of $\sqrt{2}$ in σ stemming from the two-dimensional nature of the problem.[15] On the other hand, (ϕ, ψ)-space diffusion length r_{pp} $r_{\phi\psi} = r_{xy}/\sqrt{J}$. The half-diffusion-steps thus have a length $R \cdot \sqrt{2\delta t}$,[15–19] where R is a random number from a normal distribution generated using the Box-Muller method.[20–22] The direction of the diffusion step θ_{xy} is distorted in (ϕ, ψ)-space to $\theta_{\phi\psi} = \tan^{-1}[\delta\psi/\delta\phi]$. Writing $\delta\psi$ and $\delta\phi$ in terms of total differentials, $\theta_{\phi\psi}$ can be defined in terms of the local velocity field $\theta_{\phi\psi} = \tan^{-1}[(u\delta y - v\delta x)/(u\delta x + v\delta y)]$.

Timestep independence was tested and established in the more extreme geometry (high m) cases. Infinite accelerations near corners cannot be avoided due to the use of potential flow as a model for pure electrophoretic transport. Thus if Pe/J is too large (near convex corners where fluid acceleration is highest) particles can shoot too far. When such cases are detected, we employ an adaptive integration scheme that is somewhat computationally expensive but is quite robust and need only be performed for a very small fraction of the particles.[23] This technique finds the displacement along a streamline iteratively, numerically integrating the time elapsed until it matches the timestep.

This method was validated against theory for pressure-driven flow between flat plates[24] using various values of N. Excellent agreement (shown in Fig. 2) with $\chi^2 = 0.19$ was obtained nearly independently of the choice for $N > 5000$. A value of $N = 50\ 000$ was chosen for practical computational expense while keeping statistical error very low.

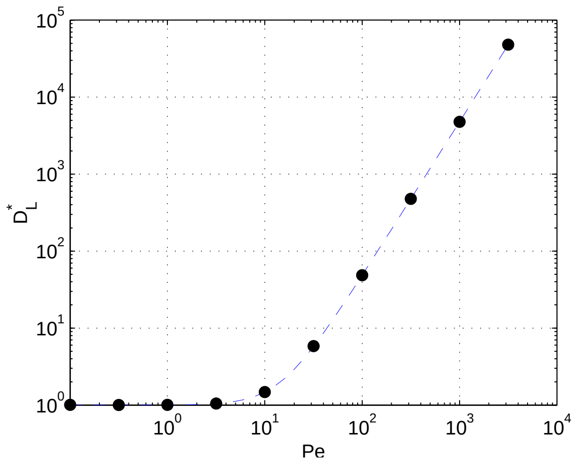

Figure 2: Comparison of simulation results and theory with $N = 50\ 000$ particles. The dashed line represents theory; $\chi^2 = 0.19$.

3 Tabulated Curve Fits to $D_L(Pe)$ Data

Below ware results for the best-fit parameters for all three curve fits, as well as the χ^2 values for each curve fit. Values for Λ for each geometry are also tabulated as a function of geometry and m.

Table 1: Fit parameters and length scales for in-line circles.

m	Λ	D_{L0}	$\sqrt{\alpha_1}$	χ_1^2	$\sqrt[n_2]{\alpha_2}$	n_2	χ_2^2	$\alpha_{3,1}$	$\sqrt{\alpha_{3,2}}$	χ_3^2
0.150	0.771	0.922	88	21	84	1.955	16	286	91	6
0.169	0.734	0.906	75	32	71	1.947	24	191	78	8
0.200	0.674	0.883	62	52	56	1.928	37	112	65	9
0.226	0.623	0.862	55	76	49	1.912	53	78	58	11
0.250	0.575	0.843	50	118	43	1.892	83	54	54	16
0.282	0.510	0.794	45	213	36	1.847	144	32	49	26
0.300	0.474	0.774	44	266	33	1.808	163	26	48	22
0.339	0.397	0.726	42	458	25	1.692	229	16	48	18
0.350	0.373	0.703	42	527	22	1.640	227	14	48	13
0.357	0.358	0.690	42	586	21	1.606	244	12	49	12
0.395	0.278	0.657	44	865	14	1.454	178	9	52	25

Table 2: Fit parameters and length scales for staggered circles.

m	Λ	D_{L0}	$\sqrt{\alpha_1}$	χ_1^2	$\sqrt[n_2]{\alpha_2}$	n_2	χ_2^2	$\alpha_{3,1}$	$\sqrt{\alpha_{3,2}}$	χ_3^2
0.150	0.776	0.939	90	15	86	1.962	12	342	92	4
0.169	0.741	0.921	78	21	74	1.957	16	245	80	5
0.200	0.685	0.894	64	48	58	1.927	32	118	67	6
0.226	0.638	0.864	56	70	50	1.915	48	83	59	10
0.250	0.594	0.850	52	109	44	1.889	71	58	55	14
0.282	0.536	0.807	47	179	38	1.855	119	38	52	21
0.300	0.504	0.770	45	238	35	1.820	146	29	50	19
0.339	0.436	0.750	45	371	29	1.734	199	20	51	24
0.350	0.416	0.738	45	430	26	1.685	198	18	51	17
0.357	0.404	0.728	45	452	26	1.665	192	17	52	21
0.395	0.338	0.704	47	708	18	1.505	159	12	55	36

Table 3: Fit parameters and length scales for in-line diamonds.

m	Λ	D_{L0}	$\sqrt{\alpha_1}$	χ_1^2	$\sqrt[n_2]{\alpha_2}$	n_2	χ_2^2	$\alpha_{3,1}$	$\sqrt{\alpha_{3,2}}$	χ_3^2
0.141	0.748	0.953	118	7	113	1.964	4	653	120	2
0.150	0.733	0.891	105	31	99	1.946	25	320	108	15
0.200	0.645	0.912	74	21	71	1.965	18	249	76	7
0.212	0.624	0.884	68	38	64	1.946	29	161	71	11
0.250	0.560	0.874	58	45	54	1.943	35	119	61	10
0.283	0.504	0.830	52	75	47	1.920	54	78	55	14
0.300	0.475	0.814	50	95	44	1.911	69	64	53	17
0.350	0.387	0.758	48	187	39	1.864	133	39	52	29
0.354	0.381	0.748	47	195	39	1.861	138	37	52	30
0.424	0.242	0.625	51	459	33	1.724	294	20	59	64

Table 4: Fit parameters and length scales for staggered diamonds.

m	Λ	D_{L0}	$\sqrt{\alpha_1}$	χ_1^2	$\sqrt[n_2]{\alpha_2}$	n_2	χ_2^2	$\alpha_{3,1}$	$\sqrt{\alpha_{3,2}}$	χ_3^2
0.141	0.753	0.951	119	6	116	1.971	5	739	121	2
0.150	0.738	0.951	110	6	107	1.976	5	667	111	2
0.200	0.656	0.923	75	20	71	1.952	13	242	78	5
0.212	0.637	0.916	70	17	68	1.965	13	257	72	5
0.250	0.579	0.874	59	42	55	1.941	31	125	62	9
0.283	0.532	0.833	54	70	49	1.923	51	84	57	14
0.300	0.509	0.821	52	83	47	1.919	62	73	55	16
0.350	0.444	0.780	51	137	42	1.875	90	49	55	18
0.354	0.439	0.774	50	142	43	1.882	100	49	54	22
0.424	0.359	0.710	56	276	41	1.793	176	33	63	34
0.495	0.289	0.651	75	422	43	1.636	202	30	89	33

Table 5: Fit parameters and length scales for in-line squares.

m	Λ	D_{L0}	$\sqrt{\alpha_1}$	χ_1^2	$\sqrt[n_2]{\alpha_2}$	n_2	χ_2^2	$\alpha_{3,1}$	$\sqrt{\alpha_{3,2}}$	χ_3^2
0.100	0.761	0.910	107	20	102	1.958	16	372	110	7
0.150	0.644	0.901	60	46	55	1.938	35	128	62	14
0.200	0.540	0.848	42	110	35	1.883	63	45	45	16
0.250	0.446	0.777	34	280	24	1.788	133	19	37	19
0.300	0.361	0.695	30	594	14	1.617	179	9	33	35
0.350	0.278	0.634	28	1090	8	1.483	56	5	31	272

Table 6: Fit parameters and length scales for staggered squares.

m	Λ	D_{L0}	$\sqrt{\alpha_1}$	χ_1^2	$\sqrt[n_2]{\alpha_2}$	n_2	χ_2^2	$\alpha_{3,1}$	$\sqrt{\alpha_{3,2}}$	χ_3^2
0.100	0.765	0.949	109	8	107	1.981	7	613	112	3
0.150	0.650	0.900	60	35	55	1.932	21	130	63	3
0.200	0.545	0.843	42	108	36	1.888	65	47	45	7
0.250	0.451	0.777	34	274	24	1.789	122	20	38	11
0.300	0.363	0.696	30	562	15	1.636	174	10	34	40
0.350	0.277	0.644	29	1045	8	1.488	60	6	32	254

Table 7: Fit parameters and length scales for in-phase sinusoidal channels.

m	Λ	D_{L0}	$\sqrt{\alpha_1}$	χ_1^2	$\sqrt[n_2]{\alpha_2}$	n_2	χ_2^2	$\alpha_{3,1}$	$\sqrt{\alpha_{3,2}}$	χ_3^2
0.030	0.926	1.003	953	1	961	2.019	1	10^{17}	953	1
0.060	0.830	0.973	257	7	248	1.960	6	1437	263	3
0.090	0.725	0.931	126	36	117	1.928	27	294	132	10
0.120	0.619	0.882	81	83	72	1.901	60	115	87	18

Table 8: Fit parameters and length scales for out-of-phase sinusoidal channels.

m	Λ	D_{L0}	$\sqrt{\alpha_1}$	χ_1^2	$\sqrt[n_2]{\alpha_2}$	n_2	χ_2^2	$\alpha_{3,1}$	$\sqrt{\alpha_{3,2}}$	χ_3^2
0.030	0.926	0.962	891	5	867	1.943	4	7080	918	3
0.060	0.830	0.954	247	14	236	1.949	11	1053	255	6
0.090	0.722	0.937	122	35	113	1.928	26	286	128	9
0.120	0.610	0.875	78	98	68	1.890	70	98	83	20

Table 9: Fit parameters and length scales for in-phase sawtooth channels.

m	Λ	D_{L0}	$\sqrt{\alpha_1}$	χ_1^2	$\sqrt[n_2]{\alpha_2}$	n_2	χ_2^2	$\alpha_{3,1}$	$\sqrt{\alpha_{3,2}}$	χ_3^2
0.030	0.930	0.990	1358	1	1319	1.918	1	14166	1396	1
0.060	0.842	0.975	361	5	352	1.963	4	2581	370	2
0.090	0.743	0.946	174	22	164	1.945	18	558	180	8
0.120	0.639	0.901	109	63	98	1.905	46	181	116	14

Table 10: Fit parameters and length scales for out-of-phase sawtooth channels.

m	Λ	D_{L0}	$\sqrt{\alpha_1}$	χ_1^2	$\sqrt[n_2]{\alpha_2}$	n_2	χ_2^2	$\alpha_{3,1}$	$\sqrt{\alpha_{3,2}}$	χ_3^2
0.030	0.929	0.986	1309	1	1292	1.963	1	20091	1333	1
0.060	0.840	0.974	351	8	335	1.942	5	1839	361	3
0.090	0.737	0.974	171	14	163	1.956	12	678	176	5
0.120	0.627	0.921	105	47	96	1.921	35	214	111	13

References

[1] Jeppson, R.W. *J. Fluid Mech.* **1970**, *40*, 215–223.

[2] Morton, K.W.; Mayers, D.F. *Numerical Solution of Partial Differential Equations*; Cambridge University: 1994.

[3] Ciarlet, P.G. *Introduction to Numerical Linear Algebra and Optimisation*; Cambridge University: 1989.

[4] Thom, A.; Apelt, C.J. *Field Computation in Engineering & Physics*; D. Van Nostrand: London, 1961.

[5] Press, W.H.; Flannery, B.P.; Teukolsky, S.A.; Vetterling, W.T. *Numerical Recipes in C: The Art of Scientific Computing*, 2nd ed.; Cambridge University: 1993.

[6] Lau, H.T. *A Numerical Library in C for Scientists and Engineers*; CRC: 1994.

[7] Henrici, P. *Applied and Computational Complex Analysis*; John Wiley & Sons: 1974.

[8] Floryan, J.M. *J. Comput. Phys.* **1985**, *58*, 229–245.

[9] Floryan, J.M.; Zemach, C. *J. Comput. Appl. Math.* **1993**, *46*, 77–102.

[10] Batchelor, G.K. *An Introduction to Fluid Dynamics*; Cambridge University: 2000.

[11] Driscoll, T.A. *ACM T. Math. Software* **1996**, *22*, 168–186.

[12] Driscoll, T.A.; Trefethen, L.N. *Schwarz-Christoffel Mapping*; Cambridge University: 2002.

[13] Driscoll, T.A. *Schwarz-Christoffel Toolbox for MATLAB*; `http://www.math.udel.edu/~driscoll/software/SC/`, 2003.

[14] Lingevitch, J.F.; Bernoff, A.J. *J. Fluid Mech.* **1994**, *270*, 219–249.

[15] Einstein, A *Investigations on the Theory of the Brownian Movement*; Dover: New York, 1956.

[16] Griffiths, S.K.; Nilson, R.H. *Anal. Chem.* **2000**, *72*, 5473–5482.

[17] Griffiths, S.K.; Nilson, R.H. *Anal. Chem.* **2001**, *73*, 272–278.

[18] Ghoniem, A.F.; Sherman, F.S. *J. Comput. Phys.* **1985**, *61*, 1–37.

[19] Chorin, A.J. *J. Fluid Mech.* **1973**, *57*, 785–796.

[20] Box, G.E.P.; Muller, M.E. *Ann. Math. Stat.* **1958**, *29*, 610–611.

[21] Robers, S. *J. Comput. Phys.* **1985**, *58*, 29–43.

[22] Bevington, P.R.; Robinson, D.K. *Data Reduction and Error Analysis for the Physical Sciences*, 2nd ed.; McGraw-Hill: 1992.

[23] Kirchner, J.J. Master Thesis, Univ. of Michigan Mech. Eng. Dept., 2003.

[24] Wooding, R.A. *J. Fluid Mech.* **1960**, *7*, 501–515.